

Extensional rheology of concentrated emulsions as probed by capillary breakup elongational rheometry (CaBER)

Katarzyna Niedzwiedz · Hans Buggisch ·
Norbert Willenbacher

Received: 16 February 2010 / Revised: 9 July 2010 / Accepted: 3 August 2010 / Published online: 1 September 2010
© Springer-Verlag 2010

Abstract Elongational flow behavior of w/o emulsions has been investigated using a capillary breakup elongational rheometer (CaBER) equipped with an advanced image processing system allowing for precise assessment of the full filament shape. The transient neck diameter $D(t)$, time evolution of the neck curvature $\kappa(t)$, the region of deformation l_{def} and the filament lifetime t_c are extracted in order to characterize non-uniform filament thinning. Effects of disperse volume fraction ϕ , droplet size d_{sv} , and continuous phase viscosity η_c on the flow properties have been investigated. At a critical volume fraction ϕ_c , strong shear thinning, and an apparent shear yield stress $\tau_{y,s}$ occur and shear flow curves are well described by a Herschel–Bulkley model. In CaBER filaments exhibit sharp necking and t_c as well as $\kappa_{max} = \kappa(t = t_c)$ increase, whereas l_{def} decreases drastically with increasing ϕ . For $\phi < \phi_c$, $D(t)$ data can be described by a power-law model based on a cylindrical filament approximation using the exponent n and consistency index k from shear experiments. For $\phi \geq \phi_c$, $D(t)$ data are fitted using a one-dimensional Herschel–Bulkley approach, but k and $\tau_{y,s}$ progressively deviate from shear results as ϕ increases. We attribute this to the failure of the cylindrical filament assumption. Filament lifetime is proportional to η_c at all ϕ . Above ϕ_c , κ_{max} as well as t_c/η_c scale linearly with

$\tau_{y,s}$. The Laplace pressure at the critical stretch ratio ε_c which is needed to induce capillary thinning can be identified as the elongational yield stress $\tau_{y,e}$, if the experimental parameters are chosen such that the axial curvature of the filament profile can be neglected. This is a unique and robust method to determine this quantity for soft matter with $\tau_y < 1,000$ Pa. For the emulsion series investigated here a ratio $\tau_{y,e}/\tau_{y,s} = 2.8 \pm 0.4$ is found independent of ϕ . This result is captured by a generalized Herschel–Bulkley model including the third invariant of the strain-rate tensor proposed here for the first time, which implies that $\tau_{y,e}$ and $\tau_{y,s}$ are independent material parameters.

Keywords w/o emulsions · Extensional flow · Shear rheology · Yield stress · Herschel–Bulkley model

Introduction

Emulsions are mixture of two immiscible liquids, where the droplets of one phase are suspended in a continuous phase of the second one. These apparently simple materials have found applications in many areas of our every day life, e.g. food industry, cosmetics, and pharmacy, cleaning industry and environmental technology. Quality aspects which are crucial for their applicability like: ease of use, physical stability or skin, taste, and even aesthetic perception are directly related to the rheological behavior (Wilson et al. 1998; Welin-Berger et al. 2001; Brummer and Godersky 1999; Foerster et al. 1999; Penna et al. 2001). Flow at low shear relates to physical stability (Zografis 1982; Dickinson et al. 1993; Miller et al. 1999). Medium and high shear rates

K. Niedzwiedz · H. Buggisch · N. Willenbacher (✉)
Institute of Mechanical Process Engineering and Mechanics,
Karlsruhe Institute of Technology,
76131 Karlsruhe, Germany
e-mail: norbert.willenbacher@kit.edu

K. Niedzwiedz
e-mail: katarzyna.niedzwiedz@kit.edu

correspond to product behavior during spreading or pouring processes and the extensional flow is identified with such processes as coating, extrusion, and spraying.

Emulsions are thermodynamically unstable, their production requires input of external energy. This is usually provided by mixing. The mixing conditions determine the interfacial area between two phases and accordingly the droplet size distribution. A change in the droplet size or emulsion concentration can lead to strong changes in rheological properties (Prud'homme and Khan 1996; Lee et al. 1997; Rieger 1991).

At low concentrations emulsions typically exhibit Newtonian flow behavior and as long as $Ca \ll 1$ the droplets are undeformed. Deviations from the viscosity of hard spheres suspensions are due to changes of the external flow field around a drop due to internal circulation and depend on the viscosity ratio of disperse to continuous phase η_d/η_c . This is captured by the so-called Taylor equation, but up to volume fractions of about $\phi = 0.25$ the emulsion viscosity is close to that of hard spheres suspensions (Macosko 1994). At higher concentrations differences between emulsion and suspension rheology become more and more pronounced, shear thinning occurs and the dependence of the zero-shear viscosity on volume fraction can be described phenomenological by a modified Krieger-Dougherty equation including the viscosity ratio η_d/η_c (Pal 2001). Suspensions cannot flow anymore at concentrations above ϕ_c , when particles are densely packed. For the concentrated emulsions with $\phi > \phi_c$ this is different due to droplet deformability. Steady shear flow behavior is characterized by strong shear-thinning and an apparent yield stress. In small amplitude oscillatory shear such emulsions behave predominantly elastic ($G' \gg G''$). Princen and Kiss proposed a model describing shear flow of such highly concentrated, monodisperse emulsions (Princen 1983; Princen and Kiss 1986, 1989). Since macroscopic deformation and flow are closely related to the deformation of individual droplets, they presume that the yield stress $\tau_{y,s}$ and static shear modulus G_0 scale with the internal Laplace pressure $2\sigma_i/d_{sv}$ of the droplets, where σ_i is the interfacial tension between the oil and water phase and d_{sv} is the droplet diameter. Furthermore, $\tau_{y,s}$ and G_0 also depend on geometrical packing, i.e., volume fraction of the disperse phase. Princen and Kiss report a value $\phi_c = 0.71$. Investigations by Ponton et al. (2001) and Jager-Lézer et al. (1998) on cosmetic w/o emulsions confirmed the predictions of Princen and Kiss. They found an agreement for the shear modulus measured for emulsions with different droplet sizes and volume fractions, but $\phi_c \approx 0.67$ was found. Mason et al. (1996) also confirmed that the yield stress of w/o emulsions scales with internal Laplace

pressure. However, they found a stronger dependence of $\tau_{y,s}$ on ϕ and a lower value $\phi_c = 0.635$.

Mason also introduced an effective volume fraction ϕ_{eff} including a thin surfactant layer on a droplet surface (Mason et al. 1996; Calderon et al. 1994). The Mason equation for the yield stress which will be used below to describe the behavior of the emulsions investigated here reads:

$$\tau_{y,s} = 0.51 \frac{2\sigma_i}{d_{sv}} (\phi_{eff} - \phi_c)^2 \quad (1)$$

Beyond that, the rheology of emulsions is modified by droplet size distribution and repulsive (steric or electrostatic) colloidal interactions (Tadros 1994; Larson 1999), e.g., for polydisperse emulsions the surface-volume mean diameter has to be used for the calculation of the internal Laplace pressure entering in Eq. 1. Moreover, additional effects can modify the flow behavior of emulsions, e.g., flocculation with the formation of a sample spanning network can give rise to a yield stress and pronounced elasticity even at a low disperse phase concentration when attractive droplet interactions dominate. It is also possible to vary emulsion rheology by modifying the continuous phase using polymeric thickeners or additional surfactants, which is commonly used in rheology of commercial emulsions (Wilson et al. 1998; Welin-Berger et al. 2001; Miller and Löffler 2006; Ghannam and Esmail 2005).

In spite of a quite good understanding of deformation and breakup of single droplets as well as emulsification phenomena in shear and elongational flows (Schubert 2005), there is not much known about elongational flow behavior of concentrated emulsions. To our knowledge the extensional rheology has not been investigated systematically so far. In contrast to the case of Newtonian fluids, for the emulsion systems there is no universal relationship between flow resistance under shear and elongational deformation. Therefore, it is important to perform elongational measurements independently.

Here, we use the capillary breakup elongational rheometer (CaBER) technique in order to characterize the elongational flow behavior of concentrated emulsions. In CaBER experiments the sample is filled between two coaxial parallel plates creating a fluid connection between them. The plates are rapidly moved apart from each other corresponding to a step strain deformation. The resulting liquid bridge deforms gradually under the action of visco-elastic and capillary forces, contracts, and finally breaks. The advantage of this method is that it is fast, straightforward and requires only a small amount of probing sample ($V < 0.1$ ml). It can be applied to fluids with viscosities

between 50 and 10^4 m Pa s. Investigations on extensional viscosity using the CaBER technique started with dilute and semi-dilute polymer solutions. Such solutions form cylindrical filaments and their diameter decays exponentially in time (Kheirandish et al. 2008; Oliveira et al. 2006; Stelter and Brenn 2000), i.e., they exhibit uniform deformation at a constant strain rate and a characteristic elongational relaxation time λ_E can be extracted directly from the transient filament diameter $D(t)$ (Rodd et al. 2005; Bazilevskii et al. 1997, 2001). Experimental results show that, in the dilute region relaxation time probed by CaBER is equal to the longest shear relaxation time, $\lambda_S = \lambda_E$. For semi-dilute solutions of linear, flexible polymers, but also for polyelectrolyte complexes and commercial acrylic thickeners formation of exponentially decaying, cylindrical filaments is observed, but elongational relaxation time is much lower than shear relaxation time, $\lambda_E \ll \lambda_S$ and the interpretation of λ_E is still under discussion (Kheirandish et al. 2009; Clasen et al. 2006; Willenbacher et al. 2008). In general, fluid filaments are not cylindrical and their diameter does not decay exponentially, i.e., neither strain nor strain rate are constant or uniform throughout the filament. This has been confirmed experimentally (Kheirandish et al. 2009; McKinley 2005; Tiwari et al. 2009; Niedzwiedz et al. 2009) as well as by theoretical calculations and numerical simulations (Renardy 2002; Renardy and Renardy 2004; Yildirim and Basaran 2001; Doshi et al. 2003; Webster et al. 2008). Even in the case of Newtonian liquids thinning is inhomogeneous, filament shape is slightly concave but its diameter decreases linearly in time and numerical solutions for specified boundary conditions allow for determination of η_E directly from $D(t)$ (McKinley 2005; McKinley and Tripathi 2000). Capillary thinning experiments performed for power-law and plastic fluids provide filaments with highly non-uniform shapes (McKinley 2005; Tiwari et al. 2009; Niedzwiedz et al. 2009). Thinning often takes place only within a restricted volume of the filament around the neck, and is hardly visible beyond this region. In such cases, it is not sufficient to measure the decay of the midpoint diameter $D(t)$ and the filament lifetime t_c , but time evolution of full filament profiles needs to be analyzed and it has been shown, that the time evolution of filament curvature at the neck $\kappa(t)$, its maximum value $\kappa_{max} = \kappa(t = t_c)$, and the region of deformation l_{def} are appropriate parameters for characterization of non-uniform filament thinning (Niedzwiedz et al. 2009).

In this paper, we discuss the elongational flow behavior of w/o emulsions. Droplet volume fraction is varied in a broad range from semi-concentrated well below the critical volume fraction ϕ_c up to highly concentrated

close to unity. Variation of ϕ in this range corresponds to a variation of the rheological signature from purely shear thinning to strongly elastic behavior and the occurrence of an apparent yield stress in shear flow. The effect of volume fraction, droplet size, and continuous phase viscosity on time evolution of filament shape in CaBER experiments has been investigated. The subsequent variations in extracted characteristic parameters $D(t)$, filament lifetime t_c , the maximum curvature at the neck κ_{max} and deformation length l_{def} are discussed. Furthermore, we point at correlations existing between shear and elongational flow behavior. Finally, we present a method to determine the elongational yield stress of concentrated w/o emulsions, which can also be applied to other soft matter with an apparent yield stress.

Materials

Raw materials and preparation methods

There were two different procedures to produce the samples. In a first set of experiments we have worked with a commercial cosmetic emulsion. The sample is characterized by $d_{sv} = 0.9 \mu\text{m}$, $\phi = 0.75$ and continuous phase viscosity $\eta_c = 22$ m Pa s (at $T = 20^\circ\text{C}$). This was used as a basis to create samples with other concentrations. Lower concentrations were obtained by diluting with paraffin oil (of the same viscosity) and by adding distilled water we could increase the disperse volume fraction (sample of series A1). These emulsion mixtures were shaken for 24 h at 3,500 rpm. Thus, we have produced the samples with ϕ in a range from about 0.5 up to 0.9. One should note that neither dilution nor

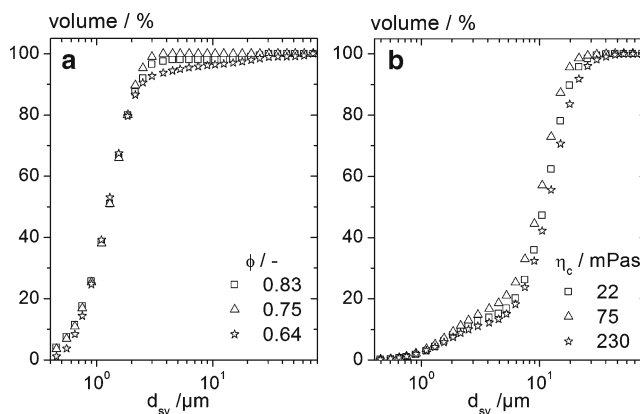


Fig. 1 Comparison of particle size distribution for the representative samples from series A1 (a) and series B2 (b)

concentration has a remarkable effect on the droplet size distribution, as shown in Fig. 1. In addition, by dilution of the commercial emulsion with high viscosity paraffin oil ($\eta_c = 230$ m Pa s) we could make a second group of samples—series A2—for which ϕ and η_c vary simultaneously. The disadvantage of this method is that η_c is related to the degree of dilution and it increases non-linearly with decreasing ϕ . Diluting sample from 0.75 up to 0.38 viscosity changes from 22 to 152 m Pa s. A third group of samples, series A3, was created by dilution of the commercial sample down to $\phi = 0.45$ using mineral oils of different viscosities, resulting in a set of samples of constant concentration, but η_c varying from 71 to 261 m Pa s.

Another set of samples (series B1) was emulsified by ourselves using a simplified recipe including only distilled water, oil, and emulsifier, without using any other additives. The oil phase consisted of a paraffin oil with $\eta_c = 230$ m Pa s and the water droplet volume fraction was chosen to be $\phi = 0.7$. Polyglyceryl-3 Polyricinoleate (Imwitor®R 600, SASOL, Germany), also known as E476 (Wilson et al. 1998), was chosen as an emulsifier. Polyglyceryl-3 Polyricinoleate is a non-ionic, PEG-free emulsifier, made by esterification of polyglycerin, and plant-derived condensed castor oil fatty acids. Its hydrophilic lipophilic balance value is $HLB = 4$. Thus, it is a powerful w/o emulsifying agent and is especially suitable for low viscosity and highly concentrated emulsions.

The emulsification procedure was as follows. The oil phase was mixed with emulsifier and heated to $T = 70^\circ\text{C}$. The volume of added emulsifier was varied depending on the desired droplet size, and was kept between 5% and 20%, referred to the oil phase. A coarse premix emulsion was obtained by slowly adding water under blade stirring conditions (10 min at 500 rpm). The final droplet size was adjusted by further stirring of this coarse emulsion premix. Time and speed of stirring varied in the range from 5 to 30 min and from 100 to 13,500 rpm, respectively, resulting in average droplet size between 2.4 and 10.3 μm .

Finally, we have created a set of home-made samples (series B2) with different continuous phase viscosity, using paraffin oils with $\eta_c = 22$ m Pa s, $\eta_c = 230$ m Pa s, and a 1:1 mixture of these oils ($\eta_c = 75$ m Pa s). For this group, $\phi = 0.7$ and $d_{sv} \approx 5.5$ μm .

One should note that due to the relatively large droplet size most of these emulsions were not very stable. Changes in the droplet size distribution started to occur already after 3 days. Therefore, all measurements were performed within 2 days after preparation. The basic parameters for all investigated samples are summarized in Table 1.

Surface and interfacial tension

Surface and interfacial tensions were measured according to the Wilhelmy plate method using a DCAT 11EC

Table 1 Characteristic parameters for all investigated emulsion samples

	$d_{sv}/\mu\text{m}$	$\eta_c/\text{m Pa s}$	$\phi/-$
Series A1	0.9	22	0.53, 0.56, 0.60, 0.64, 0.68, 0.69, 0.71, 0.74, 0.75, 0.76, 0.78, 0.79, 0.80, 0.81, 0.83, 0.84, 0.85, 0.86, 0.88
Series A2	0.9	31 40 47 52 65 75 90 100 126 152	0.74 0.71 0.69 0.68 0.64 0.60 0.56 0.53 0.46 0.38
Series A3	0.9	71, 126, 139, 261	0.45
Series B1	2.4, 3.2, 3.7, 4.7, 5.1, 5.9, 6.4, 7.8, 8.1, 9.8, 10.3	230	0.70
Series B2	5.6 5.7 5.0 5.9	22 22 75 230	0.70

tensiometer (Dataphysics, Germany; McClements 1999). Measurements were performed at room temperature. The results obtained for the surface tension of the samples of different droplet size and concentrations are nearly identical (we have measured all samples except these with $\phi > 0.75$, here the apparent yield stress prevents usage of this technique). The average value measured for samples from series A and series B are nearly identical and is $\sigma_s = 36 \pm 2$ mN/m. This also corresponds to the interfacial tension σ_i between oil and aqueous phase. However, by adding emulsifier the interfacial tension is strongly reduced. Already 5% of Imwitor[®]R 600 given to the oily phase is sufficient to lower σ_i by one order of magnitude. The interfacial tension for samples from series B is $\sigma_i = 3.6 \pm 0.4$ mN/m and stays unchanged with further increase of emulsifier concentration. For the commercial sample (series A) σ_i is even lower, $\sigma_i = 2.6 \pm 0.3$ mN/m.

Droplet size distribution

The droplet size distribution was measured by static light scattering in the Fraunhofer diffraction limit using a HELIOS device with wavelength of 632.8 nm (Helium–Neon Laser Optical System, Sympatec, Germany). The volume fraction of particles with diameter d_i is obtained from the angular dependence of scattered light intensity. From this we calculate the number fraction f_i of particles with d_i (Leschonski 1984), and the surface-volume mean diameter, d_{sv} is given by:

$$d_{sv} = \frac{\sum f_i d_i^3}{\sum f_i d_i^2} \quad (2)$$

The sets of series A samples are characterized by small droplets ($d_{sv} = 0.9$ μm) and a narrow distribution. On the other hand, the samples from series B have bigger size and their distribution is slightly broader (see Fig. 1).

Experimental

Shear rheology

Shear experiments were performed using a controlled stress rheometer (HAAKE Rheostress RS 150, Thermo HAAKE, Germany). All emulsions were measured at $T = 20^\circ\text{C}$ using cone-plate geometry (diameter

cone angle 50 mm/ 1°). The gap distance between cone and lower rheometer plate was 0.053 mm, which is at least five times larger than the largest d_{sv} . There was no indication of slip effects on the plate surface and the measurements on a given emulsion were well reproducible when samples were newly loaded to the rheometer. For the determination of the apparent yield stress we have performed creep tests, where τ increased logarithmically from 0.1 to 50 Pa, for samples with low internal phase concentration ($\phi < 0.75$) and from 0.1 to 500 Pa for samples with higher concentrations. The sampling time in each single measurement was 900 s.

Extensional rheology

Elongational experiments were performed on a CaBER device (CaBER_1, Thermo HAAKE, Germany). The experiments were carried out at room temperature. The default plate separation distances were $h_0 = 3.00$ mm and $h_f = 16.64$ mm, i.e., Hencky strain, $\varepsilon = 1.71$. The plates were separated in the cushioned stretching profile within $t_s = 40$ ms. The subsequent filament thinning process was captured by a high-speed camera with a sampling speed of $1,000$ frames per second, the telecentric optics ensured spatial resolution of 16.13 μm and image analysis provided the transient filament diameter over the full filament length (Niedzwiędz et al. 2009). Different settings for h_0 , h_f , and t_s have been chosen in the experiments used to determine the elongational yield stress. Rheological results obtained from CaBER experiments must be carefully considered with respect to the preconditioning of the samples including the appropriate choice of the stretch parameters in the initial step strain. This is particularly true for complex fluids like wormlike micellar solutions, polymer blends (Miller et al. 2009) and also emulsions (Niedzwiędz et al. 2009). Miller et al. (2009) observe a change in droplet diameter of the investigated polymer blends when a critical capillary number is exceeded. For the emulsions investigated here the capillary number, $\text{Ca} = \eta_c \dot{\varepsilon} d_{sv} / 2\sigma_i$ in the initial step strain of the CaBER experiment varies between 10^{-4} and 10^{-2} depending on the continuous phase viscosity and droplet size. Therefore, we do not expect droplet deformation or breakup to be relevant during filament formation. This has been confirmed by droplet sizing experiments on selected samples before and after CaBER experiments. Within the accuracy of the HELIOS device we did not detect any significant differences in the droplet size.

Results and discussion

Shear measurements

Disperse volume fraction

The measured flow curves for the samples of series A1 are shown in Fig. 2. The emulsions exhibit an apparent yield stress $\tau_{y,s}$ and shear thinning behavior. Obviously, $\tau_{y,s}$ as well as the degree of shear thinning increases with increasing ϕ . At low concentrations only negligibly small yield stresses are measured, but at $\phi \approx 0.66$ an abrupt increase of $\tau_{y,s}$ is observed. Quantitative analysis of the flow curves was done by fitting experimental results with the Herschel–Bulkley model:

$$\tau = \tau_{y,s} + k\dot{\gamma}^n \quad (3)$$

In the fit procedure we have allowed for a variation of all three parameters, $\tau_{y,s}$, k , and n . The results obtained for $\tau_{y,s}$, k , and n are shown in Tables 2 and 3. These data will be discussed in more detail along with the results from the elongational experiments presented below.

Droplet size and continuous phase viscosity

Emulsions of series B1 with varying d_{sv} but constant $\phi = 0.7$ exhibit similar rheological features as the samples of series A with $\phi > \phi_c$. The apparent yield stress and the degree of shear thinning weakly decrease with increasing d_{sv} according to the respective change in internal Laplace pressure. The absolute values within this series differ by less than one decade. The resulting

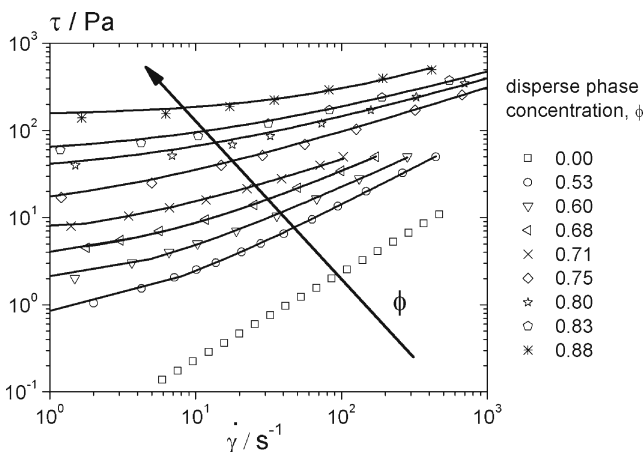


Fig. 2 Flow curves measured for the w/o emulsions from series A1. Solid lines represent fit results with Herschel–Bulkley model, Eq. 3

Table 2 Comparison of the fit parameters obtained for the power-law model from shear and elongational experiments for emulsion series A1 with $\phi < \phi_c$

ϕ	Shear experiment		Elongational experiment	
	n	k/Pa s ⁿ	n	k/Pa s ⁿ
0.64	0.80	0.79	0.99	0.17
0.60	0.80	0.52	0.99	0.14
0.56	0.81	0.41	0.93	0.15
0.53	0.85	0.29	0.95	0.11

$\tau_{y,s}$ obtained from fitting the data with the Herschel–Bulkley model (Eq. 3) agree reasonably well with the predictions of Eq. 1.

We have also investigated two sets of emulsions with varying continuous phase viscosity, namely series A3 ($\phi = 0.45$, $d_{sv} = 0.9 \mu\text{m}$) and B2 ($\phi = 0.70$, $d_{sv} \approx 5.5 \mu\text{m}$). As expected, viscosity and degree of shear thinning are larger for the series with higher ϕ than that for the low ϕ series, but the shape of the $\eta(\tau)$ curves is independent of η_c , which is just a constant prefactor in the $\eta(\tau)$ curves.

Elongational measurements

First, qualitative analysis of elongational flow properties can be done comparing the filament shapes captured by the high-speed camera. Image sequences showing effects of disperse phase concentration on filament thinning are presented in Fig. 3. Typically for the yield stress and power-law fluids the thinning process starts slowly and rapid deformation occurs only shortly before breakup. Thus, the image sequences are compared with respect to the filament lifetime, t_c . It is clearly visible that the filament profiles of the samples with higher disperse phase concentration exhibit stronger necking and the thinning process takes place only in a narrow region around a well-defined necking point for $\phi > \phi_c$. As the disperse volume fraction decreases the thinning region becomes larger, the filament curvature decreases and for $\phi < \phi_c$ essentially resembles the shape observed for the pure continuous phase. At that point, one should note that for the samples with $\phi \geq 0.8$ the existence of high apparent yield stresses prevents the self-thinning process under given experimental conditions. Instead, the stretched droplet adapts its static equilibrium shape.

To get more accurate information on filament thinning we have analyzed full image sequences and observed the time evolution of filament diameter over their full height. The images were analyzed based on light intensity scans, automatically recognizing the filament edges and calculating the diameter line by line

Table 3 Comparison of the fit parameters obtained for the Herschel–Bulkley model from shear and elongational experiments for emulsion series A1 with $\phi > \phi_c$

ϕ	n	Shear experiment		Elongational experiment	
		τ_y/Pa	$k/\text{Pa s}^n$	τ_y/Pa	$k/\text{Pa s}^n$
0.78	0.41	21.0	12.1	35.0	15.5
0.76	0.47	18.0	9.4	30.0	17.2
0.75	0.62	13.0	3.2	27.0	7.9
0.74	0.51	11.0	6.4	18.0	7.7
0.71	0.64	4.0	2.4	4.0	6.4
0.69	0.60	3.0	3.2	3.0	6.0
0.68	0.73	2.5	1.1	2.5	2.8

at any filament height as described in Niedzwiedz et al. (2009). The representative results for transient filament diameter evaluated at the neck point are shown in Fig. 4. Obviously, the neck diameter immediately before failure is always around 20 μm corresponding to the optical resolution of the objective used in this series of experiments. For $\phi < \phi_c$ the filament lifetime t_c is short and varies in a narrow range between 30 and 70 ms, but for $\phi > \phi_c$ increases strongly up to several seconds. Furthermore, also the curvature of $D(t)$ curves changes at ϕ_c . Below this value, the neck diameter decays smoothly, but for $\phi > \phi_c$ a sharp downward bent is visible in the $D(t)$ curves.

The low-concentrated samples ($\phi < \phi_c$) do not exhibit a yield stress or its value is very small and in CaBER experiments their filament curvature is negligibly small. Therefore, we use a simple analytical model to describe the time evolution of the neck diameter McKinley (2005):

$$D(t) = D_0 \Phi(n) \frac{\sigma_s}{k} (t_c - t)^n \tag{4}$$

This equation has been derived for power-law fluids based on a one-dimensional analysis of the CaBER experiment assuming uniform deformation of cylindrical

cal filaments and a negligible axial stress $\tau_{xx} \approx 0$. The involved parameters are similar as in the Herschel–Bulkley model, i.e., k is the consistency factor and n is the power-law coefficient, D_0 is the initial filament diameter, and $\Phi(n) = 0.071 + 0.239(1 - n) + 0.548(1 - n)^2$ is a numerical factor depending on the degree of shear thinning.

In Fig. 5 we compare the experimentally determined $D(t)$ curves with model predictions based on Eq. 4 and the corresponding model parameters are summarized in Table 2. We have calculated $D(t)$ using the parameters k and n obtained from independent shear experiments and to a first approximation these calculations agree quite well with the experimental data, i.e., the same power-law parameters can be used to describe shear as well as extensional flow. This is of course not trivial and as can be seen from Fig. 5 the agreement between experiment and model calculations can be further improved, especially for the samples with higher droplet concentration, if k and n are treated as free fit parameters.

Nevertheless, the power-law model starts to fail at $\phi \approx 0.65$, which is not surprising since $\tau_{y,s}$ is no longer negligible. In order to describe the filament thinning of the higher concentrated emulsions we need to account for $\tau_{y,s}$. An according solution was recently suggested

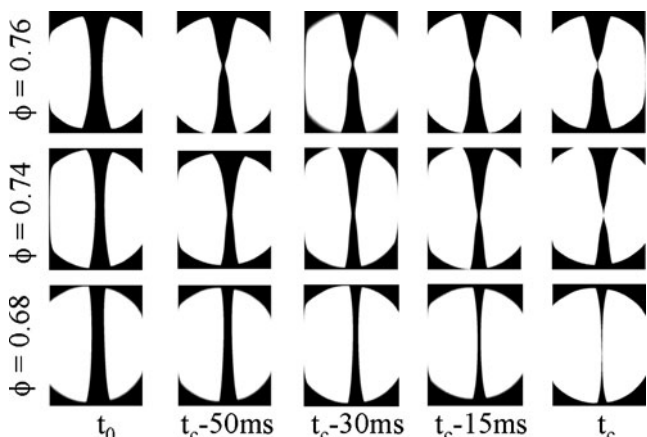


Fig. 3 Filament profiles formed during capillary thinning in CaBER experiments for samples of different disperse phase concentration

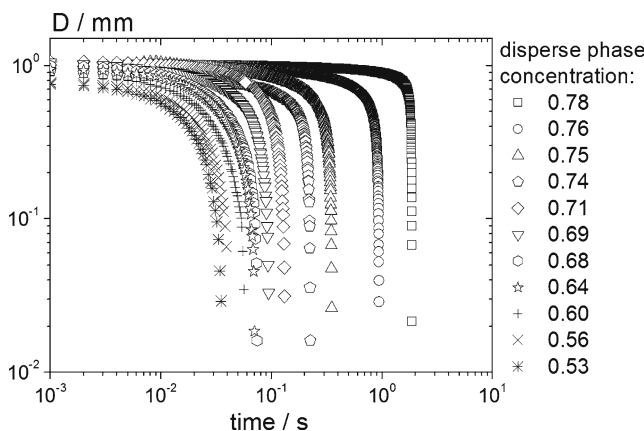


Fig. 4 Transient diameter measured at the neck of the filament for the w/o emulsions from series A1

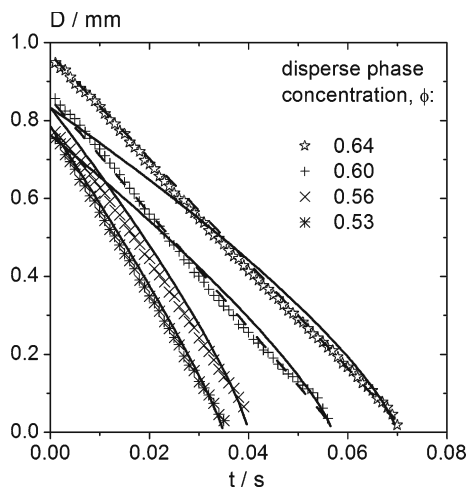


Fig. 5 The transient diameter at the neck measured for low concentrated emulsions from series A1. The *solid lines* represent the prediction of a one-dimensional power-law model (Eq. 4) using parameters n and k independently obtained from shear experiments. The *dashed lines* show a fit of Eq. 4 to the experimental data for $\phi = 0.6$ and 0.64 where k and n are varied independently

by Tiwari et al. (2009) investigating capillary thinning of carbon nanotube suspensions. Based on the constitutive model of Herschel and Bulkley and again assuming that the self-thinning of filaments in CaBER experiments is quasi one-dimensional, i.e., filaments are cylindrical and thin uniformly. Assumed that there is no flow in the end regions of filament thread and that $\tau_{xx} \approx 0$ they obtained the following differential equation for the transient filament diameter:

$$3^{(n+1)/2} k \left(-\frac{2}{D} \frac{dD}{dt} \right)^n + \sqrt{3} \tau_{y,s} - \frac{2\sigma_s}{D} = 0 \tag{5}$$

This equation is derived on the basis of the following tensorial form of the Herschel–Bulkley model (Alexandrou et al. 2003; Basterfield et al. 2005; Coussot and Gaulard 2005; Castro et al. 2010):

$$T = 2 \left[\frac{\tau_{y,s}}{\sqrt{|\text{II}|}} + k \left(\sqrt{|\text{II}|} \right)^{n-1} \right] D \tag{6}$$

where T is the extra-stress tensor, D the strain-rate of strain tensor. In simple shear flow, the second invariant of D , $\text{II} = \frac{1}{2} [(\text{tr} 2D)^2 - \text{tr} (2D)^2] = -\dot{\gamma}^2$ and Eq. 6 reduces to Eq. 3.

In uniaxial elongation $\text{II} = -3\dot{\epsilon}^2$ and for $\dot{\epsilon} > 0$ the first normal stress difference reduces to:

$$\tau_{xx} - \tau_{yy} = \sqrt{3} \left(\tau_{y,s} + k \left(\sqrt{3}\dot{\epsilon} \right)^n \right) \tag{7}$$

Where $\dot{\gamma}$ and $\dot{\epsilon}$ are the shear and elongation rate, respectively.

This corresponds to a constant relationship between elongational and shear yield stress:

$$\tau_{y,e} = \sqrt{3} \tau_{y,s} \tag{8}$$

This relationship tacitly assumes that the extra-stress tensor is independent of the third invariant of the strain-rate tensor $\text{III} = \det 2D$ and according to the references mentioned above Eq. 6 seems to hold for plastic solids or pastes with very high yield stresses. The validity of this assumption for the emulsions investigated here will be discussed in more detail below.

Figure 6 compares the experimental $D(t)$ curves for the higher concentrated emulsions $\phi > \phi_c$ with model predictions based on Eq. 5. Obviously, this simplified model describes the experimental data very well. In the fitting procedure n was fixed to the value determined from shear experiments and $\sigma_s = 36$ mN/m was taken from surface tension measurements. The apparent yield stress $\tau_{y,s}$ and k were left as free parameters.

For the samples with $\phi \approx \phi_c$ we obtain similar values for $\tau_{y,s}$ as in shear experiments, but k values are clearly higher than in shear experiments. At higher concentrations $\phi \geq 0.74$, where the samples exhibit pronounced yield stress in shear experiments and strong filament curvature in elongational experiments, the fit results show severe discrepancies also for $\tau_{y,s}$. In this concentration range the yield stress values extracted from elongational experiments seem to be about a factor of two higher than in shear experiments (see Table 3).

We attribute these deviations between experiment and model prediction to the slender filament approximation. Pronounced necking is observed above ϕ_c and

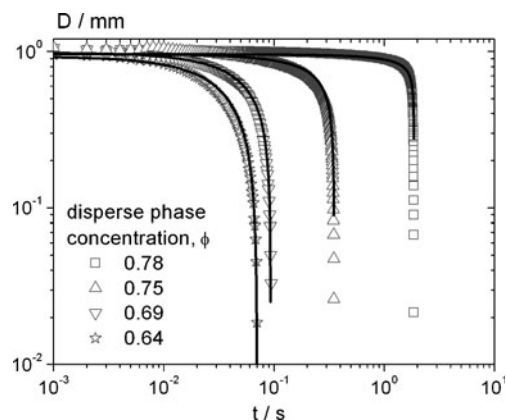


Fig. 6 The transient diameter at the neck measured for the representative samples from series A1. The *solid line* represents fit with the Herschel–Bulkley model, Eq. 5

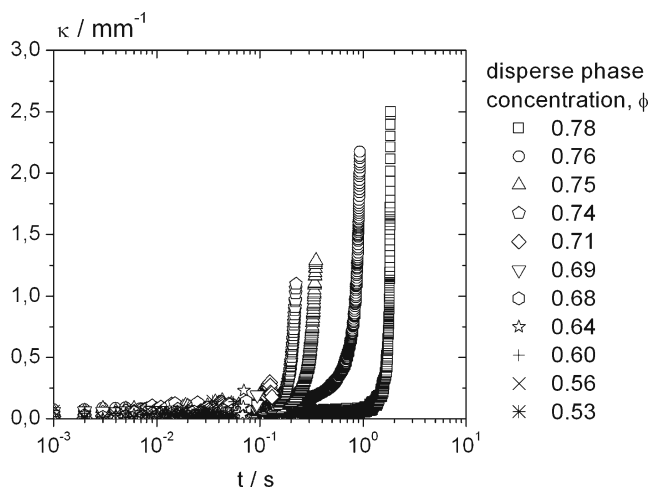


Fig. 7 Transient curvature measured at the neck of the filament for the w/o emulsions from series A1

the filaments exhibit a strongly non-uniform thinning restricted to a small region around the neck (see Fig. 3). Data presented in Fig. 7 show that the curvature at the neck increases strongly upon filament thinning. Thus, we suppose that a better description of CaBER experiments for yield stress fluids requires numerical simulation of the full, three-dimensional flow problem with appropriate boundary conditions. This is outside the scope of this paper, but in the following we will systematically discuss the effect of emulsion parameters ϕ , d_{sv} , η_c , and finally $\tau_{y,s}$ on filament thinning and in particular on filament lifetime t_c , the maximum curvature at the neck κ_{max} , and deformation length l_{def} . Finally, we will propose a new approach for a direct determination of the extensional yield stress based on CaBER experiments.

Disperse volume fraction

Figure 8 compares the results obtained for the characteristic parameters, t_c , κ_{max} , and l_{def} measured in elongational experiments upon variation of disperse volume fraction. Although there are only minor changes in the initial filament diameter, the filament lifetime strongly changes with disperse volume fraction. We can clearly distinguish two different regions. For the samples with low concentration, $\phi < 0.66$, the filaments are rather unstable, their lifetime is relatively short, on the order of tenths of milliseconds, at volume fractions $\phi > \phi_c$ filaments become much more stable and a rapid increase of t_c up to several seconds is observed. Concerning κ_{max} , again a crossover is observed at $\phi = \phi_c$. For $\phi < \phi_c$, κ_{max} is nearly constant at the level of $\approx 0.04 \text{ mm}^{-1}$, and above ϕ_c it strongly increases.

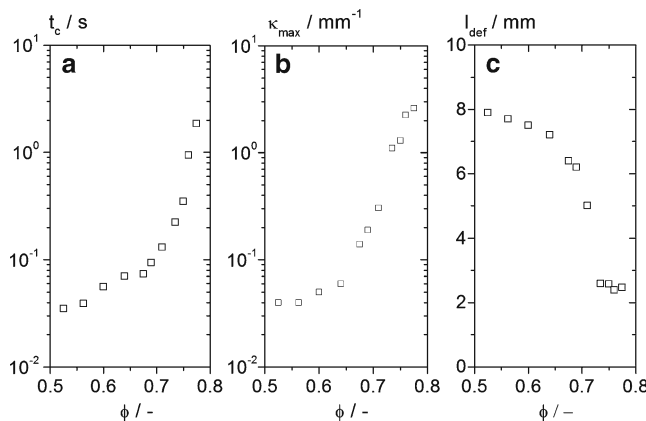


Fig. 8 Influence of dispersed volume fraction on filament life time (a), maximum filament curvature (b), and region of deformation (c). The presented results are for the emulsions from series A1

Accordingly, the region of deformation also varies. At low ϕ , where the filament thins, at its full length (as it is observed for the pure continuous phase) l_{def} stays at its maximal level. Increasing concentration above ϕ_c leads to an abrupt decrease of deformed area.

Droplet size and continuous phase viscosity

Droplet size has a significant influence on the shear flow behavior especially on the apparent yield stress of emulsions. According to Eq. 1 and as confirmed by our shear experiments $\tau_{y,s}$ is proportional to the Laplace pressure of the droplets because their deformability governs the flow behavior at such high internal phase volume fractions. CaBER experiments on samples of series B1 reveal that filament lifetime t_c and maximum curvature κ_{max} increase linearly with the internal Laplace pressure of the droplets $2\sigma_i/d_{sv}$ and hence $\tau_{y,s}$, whereas the deformation length scales as $l_{def} \propto (2\sigma_i/d_{sv})^{-1/2}$.

As already discussed above, below ϕ_c filaments thin uniformly essentially over their full length, whereas above ϕ_c strong necking occurs and filament thinning is restricted to a narrow region around the neck. Investigations on samples series A3 ($\phi = 0.45$, $d_{sv} \approx 0.9 \mu\text{m}$) and B2 ($\phi = 0.7$, $d_{sv} \approx 5.5 \mu\text{m}$) show that these characteristic features are not affected by continuous phase viscosity. Filament shape including initial filament diameter remains the same within each group of samples upon changing η_c . The maximum curvature and the deformed region are independent of η_c and t_c is proportional to η_c for both sets of emulsions. As expected, the proportionality factor is much higher for $\phi > \phi_c$ than for $\phi < \phi_c$.

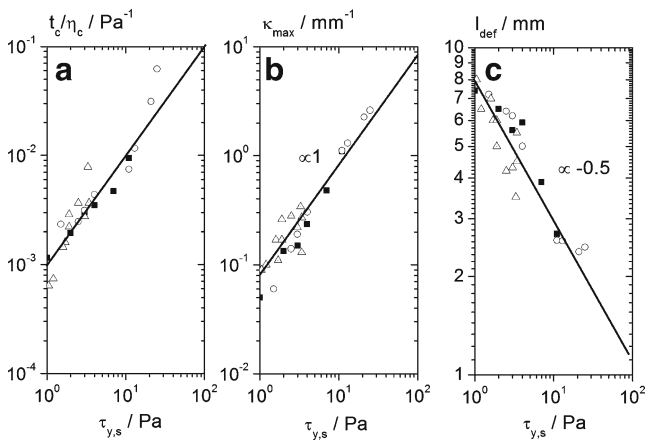


Fig. 9 Comparison of the experimental results obtained for different groups of emulsions (*open circles* series A1, *full squares* series A2, *open triangles* series B1). Figures show, respectively, influence of the apparent yield stress on filament life time (**a**), maximum filament curvature (**b**), and region of deformation (**c**). The *solid lines* show empirical scaling of the discussed parameters

Apparent yield stress

The apparent yield stress is a characteristic feature for densely packed emulsions in shear flow and in CaBER experiments the characteristic parameters are lifetime and shape of the filament. We have seen that all these parameters are strongly determined by the internal structure of the emulsion. They are especially sensitive to the variation of ϕ for $\phi > \phi_c$. Furthermore, we have observed that the changes reported in these two different experiments are correlated to each other. Filament lifetime in extensional experiments is proportional to the continuous phase viscosity. In Fig. 9 the correlation between yield stress and characteristic CaBER parameters κ_{max} , t_c/η_c , and l_{def} is shown for the three different emulsion series A1 (variation of ϕ), A2 (variation of ϕ and η_c), and B1 (variation of d_{sv}). Filament lifetime normalized by continuous phase viscosity and κ_{max} are directly proportional to the apparent shear yield stress, whereas l_{def} scales with $\tau_{y,s}^{-1/2}$.

In the following we will describe how the elongational yield stress $\tau_{y,e}$ can be directly derived from CaBER-type experiments. The method is based on earlier investigations showing, that stretched yield stress fluids can form stable bridges with lengths bigger than 2π times the radius of the cylindrical sample and that it is the yield stress which determines the onset of filament deformation (Lowry and Steen 1995; Mahajan et al. 1999). A sample droplet is placed between the plates of the CaBER device and then subsequently stretched from its initial height h_0 to different height h_f within a defined stretching time t_s . At each stretch ratio

$\varepsilon = h_f/h_0$ the filament shape is monitored for a pre-selected time t_{exp} . Here we have chosen $t_{exp} = 120$ s and if no measureable change in filament shape is detected within that time the filament is considered to be in static equilibrium. Then the Laplace pressure is determined from the radius $R(x) = D(x)/2$ and curvature $\kappa(x)$ of the filament:

$$\Delta p = \sigma_s \left(\frac{1}{R(x)} - \kappa(x) \right) \text{ with } \kappa(x) = \left| \frac{(\partial^2 R / \partial x^2)}{[1 + (\partial R / \partial x)^2]^{3/2}} \right| \tag{9}$$

But when a critical stretch ratio ε_c is exceeded, the sample starts to flow, the filament necks, and eventually breaks. Then Δp at the neck rapidly increases with time, the neck diameter decreases, and the curvature at the neck increases as shown in Figs. 4 and 7.

For a cylindrical filament in static equilibrium the force balance reduces to $-\tau_{yy} = \Delta p$. If $\tau_{xx} \approx 0$ is assumed and gravitational effects are neglected, this leads to

$$\tau_{xx} - \tau_{yy} = \Delta p \tag{10}$$

Then $\Delta p|_{\varepsilon=\varepsilon_c}$ can be identified as the elongational yield stress $\tau_{y,e}$.

The described variation in the Laplace pressure at the neck below and above ε_c is shown in Fig. 10 for the emulsion from series A1 with $\phi = 0.75$ and $\tau_{y,s} = 13$ Pa. As already mentioned in the experimental section as well as in (Niedzwi edz et al. 2009) the choice of the

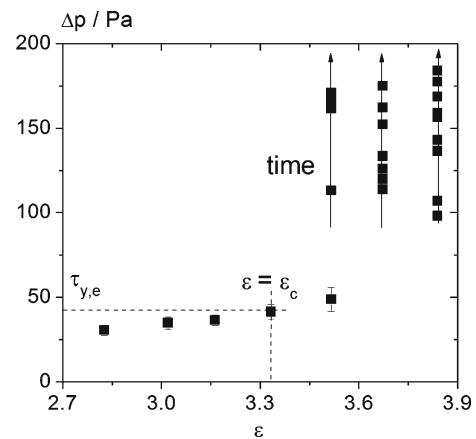


Fig. 10 Laplace pressure obtained from the shape of a liquid thread in static equilibrium at different ε . Above a critical stretch ratio ε_c the Laplace pressure exceeds the value of the elongational yield stress leading to a progressive increase of Δp and thread necking. Data shown here are for the w/o-emulsion of series A1 with $\phi = 0.75$. Experimental parameters are $h_0 = 3$ mm and $t_s = 40$ ms

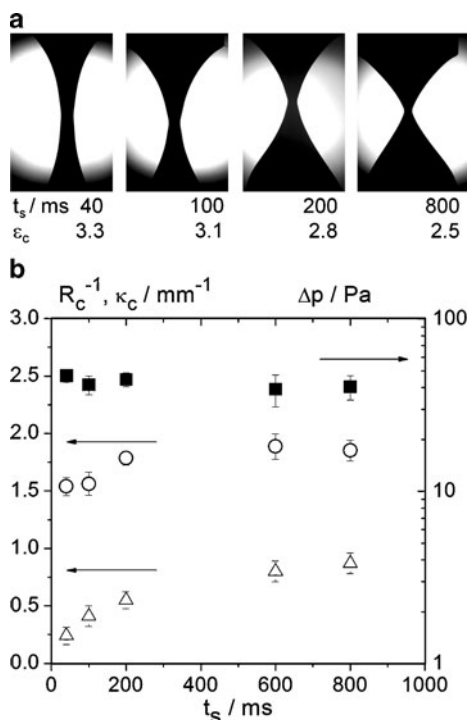


Fig. 11 a Filament profiles formed during stretching of the emulsion from series A1 with $\phi = 0.75$ in static experiments for different stretching times t_s and constant $h_0 = 3$ mm, corresponding ε_c values are also given. **b** Critical Laplace pressure Δp for $\varepsilon = \varepsilon_c$ (closed squares) and corresponding filament curvature κ_c (open triangles) and inverse radius R_c^{-1} (open circles) obtained for different stretching times t_s

initial step strain parameters can have a significant effect on the shape of the filaments and their subsequent thinning for the emulsions investigated here. The variation of the filament profile and the corresponding critical stretch ratio ε_c with stretching time t_s is shown in Fig. 11a. Obviously, ε_c decreases significantly as the stretching time t_s increases, but more importantly the filament shape also varies in a wide range. The values for $\Delta p|_{\varepsilon=\varepsilon_c}$ and the corresponding values for R_c^{-1} and κ_c are shown in Fig. 11b. Despite of the large variation in filament shape the Laplace pressure at the neck is constant within experimental uncertainty irrespective of the choice of t_s and seems to be a characteristic material parameter. Moreover, at small t_s the filament curvature is weak and the contribution of κ to Δp is only around 10%. Similar results were obtained for the other samples of series A1 with $\phi > \phi_c$. In these cases Eq. 10 is valid and $\Delta p|_{\varepsilon=\varepsilon_c}$ is a good approximation for $\tau_{y,e}$. At this point it should be noted that the cylindrical filament approximation may be applicable for the filaments in static equilibrium if the experimental conditions are chosen appropriately, but it will always fail for yield stress fluids in classical CaBER experi-

ments, since especially in the final stage of filament thinning κ strongly increases (typically more than order of magnitude, see Fig. 7) and its contribution to Δp cannot be ignored. The effect of gravity on filament stability and sagging has also to be considered and its relevance compared to surface tension is characterized by the Bond number $Bo = \rho g R^2 / \sigma_s$, where ρ is the fluid density and g is the acceleration due to gravity. A reasonable criterion for the determination of $\tau_{y,e}$ according to Eq. 10 is $Bo < 0.1$ and the initial sample volume or plate separation has to be selected accordingly. In the experiments presented here $h_0 = 2$ mm was chosen for $1 \text{ Pa} < \tau_{y,e} < 30 \text{ Pa}$ and $h_0 = 3$ mm for samples with higher yield stresses. A further reduction of accessible yield stresses could be achieved by using smaller sample volume (i.e., choosing smaller h_0). The influence of gravity may be further reduced and even yield stresses as low as 0.1 Pa should be accessible by embedding the sample into an immiscible fluid with similar density (Mahajan et al. 1999).

The experimental approach outlined above provides a unique, robust, and reliable access to the elongational yield stress of soft matter with yield stresses $\tau_y < 10^3$ Pa. Recently, Macosko and co-workers (Castro et al. 2010) have discussed the determination of the elongational yield stress of soap pastes with $\tau_y \approx 10^5$ Pa from orifice extrusion experiments, but this method is not sensitive enough for soft matter like the emulsions considered here.

The results for $\tau_{y,e}$ obtained from Eq. 10 as described above and those for $\tau_{y,s}$ extracted from the shear stress vs. shear rate data shown in Fig. 2 according to Eq. 3

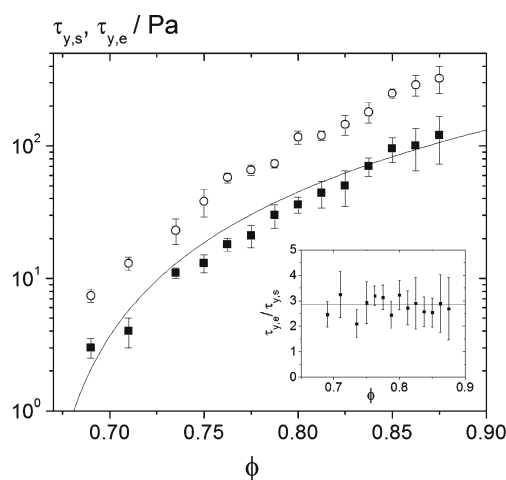


Fig. 12 Apparent elongational (open circles) and shear yield stresses (closed squares) as a function of droplet volume fraction ϕ for the w/o-emulsions of series A1. The solid line the prediction for $\tau_{y,s}$ given in Eq. 1 with $\sigma_i = 2.6$ mN/m, $d_{SV} = 0.9$ μm and $\phi_c = 0.66$. The insert shows the ratio $\tau_{y,e} / \tau_{y,s}$

are summarized in Fig. 12. The $\tau_{y,e}$ and $\tau_{y,s}$ data are shown as a function of droplet concentration ϕ and the insert shows the ratio $\tau_{y,e}/\tau_{y,s}$ for the samples of series A1. Both $\tau_{y,s}$ and $\tau_{y,e}$ increase monotonically with increasing ϕ and $\tau_{y,e}$ is always larger than $\tau_{y,s}$. The data for $\tau_{y,s}$ agree well with those predicted by Eq. 1 (Mason et al. 1996) if $\sigma_i = 2.6$ mN/m and $d_{sv} = 0.9$ μm as obtained from independent measurements are used and $\phi_c = 0.66$ is chosen. As expected the critical volume fraction is slightly higher than that for perfectly monodisperse systems, $\phi_{c,m} = 0.635$ (Mason et al. 1996). The ratio of elongational to shear yield stress is constant within experimental uncertainty and $\tau_{y,e}/\tau_{y,s} = 2.8 \pm 0.4$ is found for the emulsions series investigated here. This result is in contradiction to the $\sqrt{3}$ ratio provided by Eq. 8 based on the tensorial form of the Herschel–Bulkley model given in Eq. 6. To our knowledge such a deviation has been observed here for the first time and it seems that this constitutive equation is not sufficient to describe the yielding of soft matter and the elongational yield stress has to be treated as an independent rheological parameter. This deficiency may be due to neglecting the contribution of the third invariant of the strain-rate tensor. Therefore, we propose a generalized Herschel–Bulkley constitutive equation including III, which fulfills the general requirements for a Reiner–Rivlin fluid (Graebel 2007):

$$T = 2 \left[\frac{\tau_{y,s}}{\sqrt{|\text{II}|} + m_1 \sqrt[3]{\frac{\text{III}}{2}}} + k \left(\sqrt{|\text{II}|} + m_2 \sqrt[3]{\frac{\text{III}}{2}} \right)^{n-1} \right] D \quad (11)$$

In simple shear flow, $\text{II} = -\dot{\gamma}^2$, $\text{III} = 0$ and Eq. 11 reduces to Eq. 3. In uniaxial elongation, $\text{II} = -3\dot{\epsilon}^2$, $\text{III} = 2\dot{\epsilon}^3$, and for $\dot{\epsilon} > 0$ the first normal stress difference reads:

$$\tau_{xx} - \tau_{yy} = \frac{3\tau_{y,s}}{\sqrt{3} + m_1} + 3k \left(\sqrt{3} + m_2 \right)^{n-1} \dot{\epsilon}^n \quad (12)$$

This generalized Herschel–Bulkley constitutive model includes the material parameters m_1 and m_2 , which are irrelevant in shear experiments, but result in a nontrivial relationship between the yield stresses determined in shear and uniaxial extensional flow:

$$\tau_{y,e} = \frac{3\tau_{y,s}}{\sqrt{3} + m_1} \quad (13)$$

If the contribution of III is neglected (i.e., $m_1 = m_2 = 0$) Eqs. 11–13 reduce to Eqs. 6–8, respectively. It should be noted that Eq. 11 is just one example for a generalized Herschel–Bulkley model leading to the result, that $\tau_{y,s}$ and $\tau_{y,e}$ are independent parameters. The ex-

perimentally determined ratio $\tau_{y,e}/\tau_{y,s}$ corresponds to $m_1 = -0.73$ for the w/o emulsions investigated here. Such deviations from the standard tensorial formulation of the Herschel–Bulkley model (Eq. 6) have not been reported before. Macosko and co-workers found good agreement between the yield stress values obtained from orifice flow and shear experiments based on Eq. 6 for their soap pastes with $\tau_y \approx 10^5$ (Castro et al. 2010), also e.g. studies dealing with flow instabilities of Herschel–Bulkley fluids in complex flow kinematics analyzing experimental data on the basis of Eq. 6 did not resolve such discrepancies (Alexandrou et al. 2003; Coussot and Gaulard 2005). On the other hand, it is hard to rationalize that a unique relationship between shear and elongational yield stress like Eq. 8 should hold for all kinds of soft matter with an apparent yield stress including such a large variety of different materials like polymeric gels and networks, jammed systems like pastes or colloidal glasses, highly concentrated emulsions and foams, but also suspensions/emulsions with low internal phase volume fraction, where attractive interactions among droplets or particles lead to sample spanning network structures (Coussot 2004; Larson 1999). This topic clearly needs further investigations and the method proposed here, seems to be an appropriate starting point.

Conclusions

The flow behavior of w/o emulsions under extensional deformation has been investigated using a capillary breakup elongational rheometer. The CaBER device is equipped with an advanced image processing system including a high-speed camera and telecentric optics allowing for precise assessment of the full filament shape. The transient neck diameter $D(t)$, time evolution of the neck curvature $\kappa(t)$, the region of deformation l_{def} and the filament lifetime t_c have been extracted in order to characterize thinning and breakup of non-cylindrical filaments, typical for concentrated emulsions. Additionally, standard shear experiments were done for reference. Effects of disperse volume fraction ϕ , droplet size d_{sv} and continuous phase viscosity η_c on the flow properties have been investigated in a broad parameter range ($0.45 < \phi < 0.8$, $0.9 \mu\text{m} < d_{sv} < 10 \mu\text{m}$, $22 \text{ m Pa s} < \eta_c < 261 \text{ m Pa s}$) using well-characterized model systems.

At a critical volume fraction ϕ_c , when the droplets are densely packed and start to deform, shear as well as elongational flow properties change drastically. Shear flow curves exhibit strong shear thinning and an apparent yield stress $\tau_{y,s}$. The latter varies proportional

to the internal droplet pressure, $2\sigma_i/d_{sv}$ and $(\phi - \phi_c)^2$ as proposed earlier (Mason et al. 1996) and with $\sigma_i = 2.6$ mN/m and $d_{sv} = 0.9$ μm we find $\phi_c \approx 0.66$ for the systems investigated here. In CaBER experiments filaments exhibit sharp necking and the maximum curvature at the neck, κ_{max} , as well as t_c increase, and l_{def} decreases drastically for $\phi > \phi_c$. Shear flow curves are well described by a Herschel–Bulkley model over the entire volume fraction range. For $\phi < \phi_c$, $D(t)$ data from CaBER experiments are well described by a one-dimensional solution (cylindrical filament approximation) of the Herschel–Bulkley or power-law model using the exponent n and consistency index k from shear experiments. Around and above ϕ_c , $D(t)$ data can still be fitted using this 1–d Herschel–Bulkley approach, but first k and then $\tau_{y,s}$ progressively deviate from shear results as ϕ increases. We attribute this to the failure of the cylindrical filament assumption as necking is more and more pronounced. The curvature at the neck strongly increases with time for emulsions with $\phi \geq \phi_c$ and especially in the final stage of filament thinning the axial curvature cannot be ignored. The total filament lifetime t_c is proportional to the continuous phase viscosity η_c at low as well as at high volume fraction. Above ϕ_c , combined data for three different sets of emulsions covering a yield stress range of about two orders of magnitude show that κ_{max} as well as t_c/η_c scale linearly with $\tau_{y,s}$ and thus inversely with droplet diameter d_{sv} , which enters via its contribution to the Laplace pressure of the individual droplets, whereas l_{def} scales with $\tau_{y,s}^{-1/2}$. The elongational yield stress $\tau_{y,e}$ can be determined directly from the Laplace pressure at the critical stretch ratio at which a filament starts to thin. Experimental parameters can be set such, that the curvature of the filament in static equilibrium as well as the contribution of gravity to the stress within the filament can be neglected so that $\Delta p|_{\varepsilon=\varepsilon_c} = \tau_{y,e}$ if $\tau_{xx} = 0$ is assumed. This procedure provides a unique and reliable access to the elongational yield stress of soft matter with yield stresses $\tau_y < 10^3$ Pa. For the emulsion series investigated here, covering two orders of magnitude in the yield stress, a constant ratio $\tau_{y,e}/\tau_{y,s} \approx 3$ is found. This is captured by a generalized Herschel–Bulkley model that includes the third invariant of the strain-rate tensor, and in conclusion the elongational yield stress has to be treated as an independent fluid parameter.

Acknowledgements We would like to thank Julia Weberling and Bianca Cornehl for their help in sample preparation and performing CaBER experiments. Further, we acknowledge financial support by Beiersdorf AG and Kompetenznetz Verfahrenstechnik Pro3 e.V.

References

- Alexandrou AN, Le Menn P, Georgiou G, Entov V (2003) Flow instabilities of Herschel–Bulkley fluids. *J Non-Newton Fluid Mech* 116:19–32
- Basterfield RA, Lawrence CJ, Adams MJ (2005) On the interpretation of orifice extrusion data for viscoplastic materials. *Chem Eng Sci* 60:2599–2607
- Bazilevskii AV, Entov VM, Lerner MM, Rozhkov AN (1997) Degradation of polymer solution filaments. *Polym Sci* 39:474–482
- Bazilevskii AV, Entov VM, Rozhkov AN (2001) Breakup of an Oldroyd liquid bridge as a method for testing the rheological properties of polymer solutions. *Polym Sci A* 43:716–726
- Brummer R, Godersky S (1999) Rheological studies to objectify sensations occurring when cosmetic emulsions are applied to the skin. *Coll Surf A* 152:89–94
- Calderon FL, Stora T, Monval OM, Poulin P, Bibette J (1994) Direct measurement of colloidal forces. *Phys Rev Lett* 72:2959–2962
- Castro M, Giles DW, Macosko CW, Moaddel T (2010) Comparison of methods to measure yield stress of soft solids. *J Rheol* 54:81–94
- Clasen C, Plog JP, Kulicke WM, Owens M, Macosko C, Scriven LE, Verani M, McKinley GH (2006) How dilute are dilute solutions in extensional flows? *J Rheol* 50:849–881
- Coussot P (2004) Rheometry of pastes, suspensions, and granular materials. Applications in industry and environment. Wiley, Hoboken
- Coussot P, Gaulard F (2005) Gravity flow instability of viscoplastic materials: the ketchup drip. *Phys Rev E* 72:031409
- Dickinson E, Goller MI, Wedlock DI (1993) Creaming and rheology of emulsions containing polysaccharide and nonionic or anionic surfactants. *Colloid Surface A* 75:195–201
- Doshi P, Suryo R, Yildirim OE, McKinley GH, Basaran OA (2003) Scaling in pinch-off of generalized Newtonian fluids. *J Non-Newton Fluid Mech* 113:1–27
- Foerster T, Waldmann-Laue M, Both W, Jassoy C (1999) Lipoprotein creams: utilization of multifunctional ingredients for the preparation of cosmetic emulsions with excellent skin compatibility. *Int J of Cosmet Sci* 21:253–264
- Ghannam MT, Esmail N (2005) Yield stress behavior for crude oil-polymer emulsions. *J Pet Sci Eng* 47:105–115
- Graebel, WP (2007) Advanced fluid mechanics Associated, Press
- Jager-Lézer N, Tranchant JF, Alard V, Vu C, Tchoreloff PC, Grossiord JL (1998) Rheological analysis of highly concentrated w/o emulsions. *Rheol Acta* 23:129–138
- Kheirandish S, Guybaidullin I, Wohlleben W, Willenbacher N (2008) Shear and elongational flow behavior of acrylic thickener solutions Part I: effect of intermolecular aggregation. *Rheol Acta* 47:999–1013
- Kheirandish S, Guybaidullin I, Willenbacher N (2009) Shear and elongational flow behavior of acrylic thickener solutions. Part II: effect of gel content. *Rheol Acta* 48:397
- Larson RG (1999) The structure and rheology of complex fluids. Oxford University Press, New York
- Lee HM, Lee JW, Park OO (1997) Rheology and dynamics of water-in-oil emulsions under steady and dynamic shear flow. *J Colloid Interface Sci* 185:297–305
- Leschonski K (1984) Representation and evaluation of particle size analysis data. *Part Part Syst Charact* 1:89–95
- Lowry BJ, Steen PH (1995) Capillary surfaces: stability from families of equilibria with application to the liquid bridge. *Proc R Soc London A* 449:411–439

- Macosko CW (1994) Rheology: principles, measurements, and applications. Wiley-VCH
- Mahajan MP, Tsige M, Taylor PL, Rosenblatt C (1999) Stability of liquid crystalline bridges. *Phys Fluids* 11:491–493
- Mason TG, Bibette J, Weitz DA (1996) Yielding and flow of monodisperse emulsions. *J Colloid Interface Sci* 179:439–448
- McClements DJ (1999) Food emulsions: principles, practice, and techniques. CRC Press, 2nd Edition
- McKinley GH (2005) Annual rheology reviews. British Society of Rheology, Aberystwyth
- McKinley GH, Tripathi A (2000) How to extract the Newtonian viscosity from capillary breakup measurements in a filament rheometer. *J Rheol* 44:653–670
- Miller D, Löffler M (2006) Rheological effects with a hydrophobically modified polymer. *Colloids Surf A* 288:165–169
- Miller D, Wiener EM, Turowski A, Thunig C, Hoffmann H (1999) O/W emulsions for cosmetics products stabilized by alkyl phosphates—rheology and storage tests. *Coll Surf A* 152:155–160
- Miller E, Clasen, Rothstein JP (2009) The effect of step-stretch parameters on capillary breakup extensional rheology (CaBER) measurements. *Rheol Acta* 48:625–639
- Niedzwiedz K, Arnolds O, Willenbacher N, Brummer R (2009) How to characterize yield stress fluids with capillary breakup extensional rheometry (CaBER)? *Appl Rheol* 19:41969
- Oliveira MSN, Yeh R, McKinley GH (2006) Iterated stretching, extensional rheology and formation of beads-on-a-string structures in polymer solutions. *J Non-Newtonian Fluid Mech* 137:137–148
- Pal R (2001) Novel viscosity equations for emulsions of two immiscible liquids. *J Rheol* 45:509–520
- Penna ALB, Sivieri K, Oliveira MN (2001) Relation between quality and rheological properties of lactic beverages. *J Food Eng* 49:7–13
- Ponton A, Clément P, Grossiord JL (2001) Corroboration of Princen's theory to cosmetic concentrated water-in-oil emulsions. *J Rheol* 45:521–526
- Princen HM (1983) Rheology of foams and highly concentrated emulsions .1. Elastic properties and yield stress of a cylindrical model system. *J Colloid Interface Sci* 91:160–175
- Princen HM, Kiss AD (1986) Rheology of foams and highly concentrated emulsions .3. Static shear modulus. *J Colloid Interface Sci* 112:427–437
- Princen HM, Kiss AD (1989) Rheology of foams and highly concentrated emulsions .4. An experimental-study of the shear viscosity and yield stress of concentrated emulsions. *J Colloid Interface Sci* 128:176–187
- Prud'homme RK, Khan SA (1996) Foams: theory, measurements and applications. Marcel Dekker Inc, New York
- Renardy M (2002) Similarity solutions for jet breakup for various models of viscoelastic fluids. *J Non-Newtonian Fluid Mech* 104:65–74
- Renardy M, Renardy Y (2004) Similarity solutions for breakup of jets of power law fluids. *J Non-Newtonian Fluid Mech* 122:303–312
- Rieger MM (1991) Stability testing of macroemulsions. *Cosmet Toiletries* 106:60–69
- Rodd LE, Scott TP, Cooper-White JJ, McKinley GH (2005) Capillary break-up rheometry of low-viscosity elastic fluids. *Appl Rheol* 15:12–27
- Schubert H (2005) Emulgiertechnik: Grundlagen, Verfahren und Anwendungen, Behr's-Verlag
- Stelter M, Brenn G (2000) Validation and application of a novel elongational device for polymer solutions. *J Rheol* 44:595–616
- Tadros TF (1994) Fundamental principles of emulsion rheology and their applications. *Colloids and Surf A: Physicochem Eng Aspects* 91:39–55
- Tiwari MK, Bazilevskii AV, Yarin AL, Megaridis CM (2009) Elongational and shear rheology of carbon nanotube suspensions. *Rheol Acta* 48:597–609
- Webster MF, Matallah H, Sujatha KS, Banaai MJ (2008) Numerical modelling of step-strain for stretched filaments. *J Non-Newtonian Fluid Mech* 151:38–58
- Welin-Berger K, Neelissen J, Bergenstahl E (2001) In vitro permeation profile of a local anaesthetic compound from topical formulations with different rheological behaviour—verified by in vivo efficacy data. *Eur J Pharm Sci* 14:229–236
- Willenbacher N, Matter Y, Gubaydullin I, Schaedler V (2008) Effect of aggregation on shear and elongational flow properties of acrylic thickeners. *Korea-Aust Rheol J* 20:109–116
- Wilson R, Van Schie BJ, Howes D (1998) Overview of the preparation, use, and biological studies on polyglycerol polyricinoleate. *Food Chem Toxicol* 36:711–718
- Yildirim OE, Basaran OA (2001) Deformation and breakup of stretching bridges of Newtonian and shear-thinning liquids: comparison of one- and two-dimensional models. *Chem Eng Sci* 56:211–233
- Zografi G (1982) Physical stability assessment of emulsions and related disperse systems—a critical-review. *J Soc Cosmet Chem* 33:345–358